

Article

# Rapid Evaluation Model of Endurance Performance and Its Application for Agricultural UAVs

Jiyu Li <sup>1</sup>, Bo Long <sup>1</sup>, Han Wu <sup>1</sup>, Xiaodan Hu <sup>1</sup>, Xu Wei <sup>1</sup>, Zhixun Zhang <sup>1</sup>, Lin Chai <sup>2</sup>, Jindian Xie <sup>3</sup> and Huilan Mei <sup>1,\*</sup>

- <sup>1</sup> College of Engineering, South China Agricultural University, Guangzhou 510642, China; lijyu@scau.edu.cn (J.L.); woushent@stu.scau.edu.cn (B.L.); wuhan@scau.edu.cn (H.W.); dann@stu.scau.edu.cn (X.H.); victoryweixu@stu.scau.edu.cn (X.W.); zhangzhixun@stu.scau.edu.cn (Z.Z.)
- <sup>2</sup> College of Information Science and Engineering, Wuhan University of Science and Technology, Wuhan 430081, China; chailin@wust.edu.cn
- <sup>3</sup> Nanxiong Jianan Agricultural Science and Technology Service Co., Ltd., Nanxiong 512400, China; xiejindian@gd-tianhe.com
- \* Correspondence: huilanmei@scau.edu.cn; Tel.: +86-135-6045-5485

**Abstract:** Current developments in agricultural aviation technology have gradually increased the requirements for the endurance of agricultural unmanned aerial vehicles (UAVs). It is significant to establish an endurance evaluation model for different types of UAVs and rationalize the battery and operating load parameters on this basis, which play an important role in improving the operational efficiency of the whole UAV. Taking the quad-rotor UAV as the research object, firstly, the structural composition of the whole UAV is studied in this paper, and then the main influencing parameters of the UAV endurance evaluation model are determined, combined with the mass distribution data of specific models. Based on the above, the hovering output power of the UAV is modularly divided, and a fast measurement method is innovatively proposed to sample and fit the power data of each module. Finally, in combination with the variation law of the lithium battery discharge time, a rapid evaluation method of the endurance time of agricultural UAVs is derived and validated by the hovering test data of the agri-drone with a standard operating load of 5 kg. The results show that the mass distribution system of the UAV has the highest percentage of operational load mass (40.45% under the standard configuration); the power distribution system has the highest percentage of motor pull curve output power (91.12% under the standard configuration); the maximum error of the surface verification point in the validation experiment is 2.73%, and the model is of relatively high accuracy. The modeling idea and the supporting module power rapid measurement method can quickly model and evaluate the endurance of common agricultural drones, guide reasonable matching between the battery and operating load, and are of great significance in improving UAVs' endurance and operational efficiency.

**Keywords:** electric UAV; energy; load; model; matching scheme; endurance time



**Citation:** Li, J.; Long, B.; Wu, H.; Hu, X.; Wei, X.; Zhang, Z.; Chai, L.; Xie, J.; Mei, H. Rapid Evaluation Model of Endurance Performance and Its Application for Agricultural UAVs. *Drones* **2022**, *6*, 186. <https://doi.org/10.3390/drones6080186>

Academic Editor: Abdessattar Abdelkefi

Received: 10 June 2022

Accepted: 21 July 2022

Published: 25 July 2022

**Publisher's Note:** MDPI stays neutral with regard to jurisdictional claims in published maps and institutional affiliations.



**Copyright:** © 2022 by the authors. Licensee MDPI, Basel, Switzerland. This article is an open access article distributed under the terms and conditions of the Creative Commons Attribution (CC BY) license (<https://creativecommons.org/licenses/by/4.0/>).

## 1. Introduction

Agricultural UAVs have a high degree of intelligence and strong terrain adaptability, with obvious advantages, which can not only realize the unified production management of large-area farmland through multi-machine coordination [1] but also meet the needs of small-scale operations in mountainous and hilly areas, and the operation efficiency is about 50 times that of traditional manual ways [2,3]. Agricultural drones can be applied to plant protection and application, aerial spreading, agricultural information collection, etc., and play an important role in the agricultural production process. Currently, there are many types of rotary wing plant protection UAVs, including single-rotor, quad-rotor, six-rotor, eight-rotor, etc., according to different lift structures [4]. Among them, four-rotor drones are widely used due to their simple structure and easy maintenance [5]; Based on

the power drive mode, they can also be divided into three types: electric, oil, and hybrid power [6], among which electric UAVs have more than 80% of the market because of their simple airframe structure and low manufacturing costs [7,8].

Electric agricultural drones are powered by batteries, but the energy density of current power cells is generally lower than 250 wh/kg [9], and the power conversion efficiency of matching brushless motors is generally not higher than 75% [10]; therefore, the endurance time of agricultural UAVs is commonly less than 30 min [11], and the workload is less than 20 kg [12], which makes it difficult to meet the requirements of heavy-load long-endurance operations. Although increasing the number of batteries and reducing the operational load can improve the endurance, the former increases the weight of the batteries, which results in additional energy consumption, and the latter reduces the operational sustainability. Therefore, establishing the endurance evaluation model of the agri-drones accurately and quickly, and guiding the reasonable configuration of batteries and operating loads based on the output of the model, are important ways to improve the operational efficiency of agricultural UAVs.

Current advances related to UAV endurance research are mainly focused on endurance optimization algorithms, analysis of endurance influencing factors, and energy consumption modeling [13–15]. For example, Amila Thibbotuwawa et al. conducted a study on the energy consumption of UAVs, summarized the main influencing factors of energy consumption as weather conditions, flight speed and payloads, and established a corresponding energy consumption calculation model that was not verified. Raja Sengupta et al., based on the helicopter's energy consumption calculation model, derived and validated a theoretical estimation model of the rotor UAV endurance time; however, measurement and acquisition methods of the main parameters in this model are too complicated to achieve rapid modeling, so the actual application suffers slightly. L.W. Traub verified Peukert's endurance estimation equation by wind tunnel tests, and the results showed that its estimation accuracy is high, but the establishment and derivation process of this equation is based on fixed-wing models, which is not suitable for multi-rotor UAVs, and its application is limited.

In summary, there is still no quick and reliable assessment method for the whole aircraft endurance of rotary wing UAVs with variable loads. This paper takes the common electric quad-rotor UAV as its research object. First of all, the main parameters of UAV endurance are clarified by studying the load and energy distribution characteristics of the UAV. Secondly, the total power output of the whole aircraft is divided into four modules, namely, motor pull curve power, power divider power, power meter power, and environmental impact power, and with the help of power measurement and data fitting methods, the power fitting function of each module is obtained quickly and accurately. Finally, an endurance evaluation model of agricultural UAVs is established by combining the module power fitting function and lithium battery discharge law and verified by experiments. The results show that the model can accurately output the hovering endurance time of the electric UAVs under the different battery and operating load configurations.

Measurement methods and modeling ideas involved in the modeling process, with good portability, can be applied to different types of agricultural drones. The developed model, in addition to being used for UAV endurance evaluation, can also be associated with the liquid spraying time model to achieve the best match between endurance and effective operation time, which plays an important role in improving operational efficiency and reducing operating costs.

## 2. Materials and Methods

### 2.1. UAV Load Distribution Characteristics

The take-off mass of electric multi-rotor UAVs is expressed as  $W_T$  [16], which is composed of the fuselage structure mass  $W_1$ , power unit mass  $W_2$ , battery mass  $W_3$ , and workload mass  $W_4$ . The relationship between various mass parameters is:

$$W_T = \sum_{i=1}^4 W_i. \tag{1}$$

Taking the AX-1000 UAV as an example, its specific performance parameters are shown in Table 1. The mass distribution under different loads is shown in Figure 1.

Table 1. AX-1000 UAV configuration parameters.

Model/Parameter	Rack	Motor	ESC	Propeller	Section Board	Empty Weight	Maximum Weight	Standard Payload
AX-1000		Sunnysky 6215/350 kV	Hobbywing 80 A/120 A MAX	Sunnysky 22 inch/22 × 6.6	EFT-V3/12S200A	5 kg	17 kg	5 kg

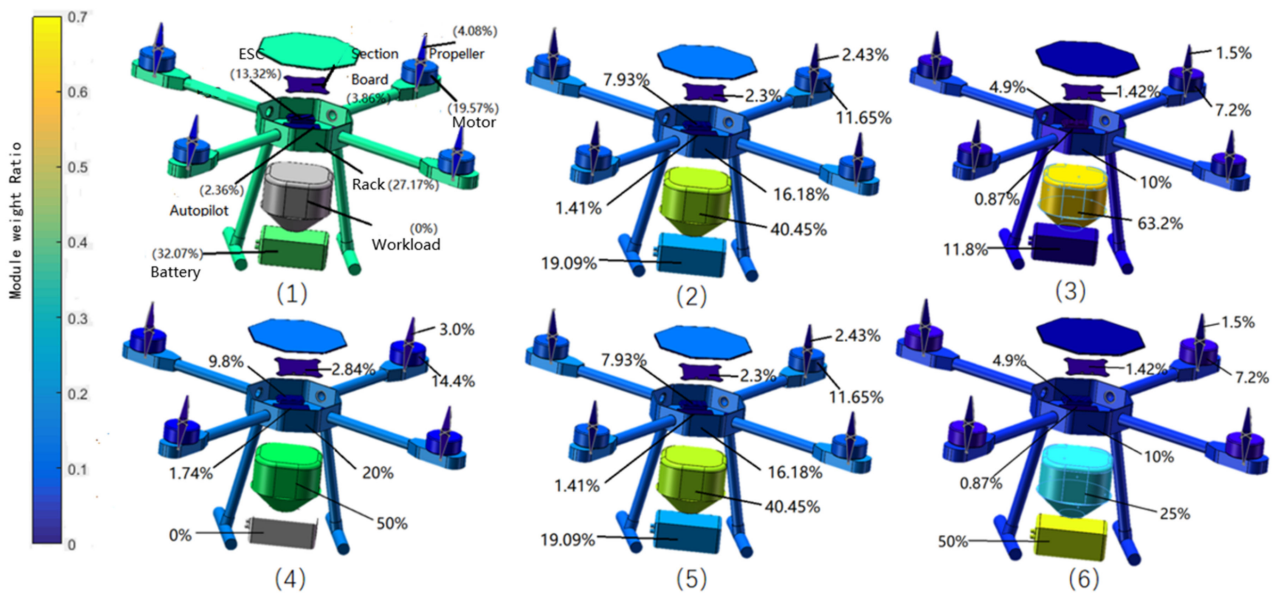


Figure 1. Vary load body mass distribution. Note: Figure (1–3), given the battery weight, increase the operating load. Figure (4–6), given the operating load, increase the battery weight.

As can be seen from Figure 1, when the given battery mass and the workload rises from 0 to the maximum (9.64 kg), the three modules with the largest mass percentage change are the operating load (0% to 63.2%), power system (36.97% to 22.1%), and battery (32.07% to 11.8%). Under the standard operating load, when the battery mass rises from 0 to the maximum (7 kg), the three modules with the largest mass percentage change are the battery (0% to 41.18%), operating load (50% to 29.41%), and power system (27.2% to 13.6%).

In conclusion, when the UAV load state is changed, the mass ratio of battery, operational load, and power system changes the most. For a given UAV configuration, the power system mass is unchangeable, so the battery mass and operational load are used as the main influencing parameters of the UAV endurance model.

## 2.2. Power Distribution Characteristics of Electric Quadrotors

From the principle of electric UAV composition [17–19], it is clear that the motor, ESC (Electronic Speed Control), paddle, and battery provide the power output for the UAV system together, and its total output power can be expressed by the motor pull curve power  $P_1$ , which is affected by the change of motor output pull  $T$  such as the power divider power  $P_2$  and power meter power  $P_3$ , and belongs to the dynamic power module. The flight control, powered by the BEC (Battery Elimination Circuit) independently, is a static power module. According to the actual parameters of flight control and the operating environment, the specific value of its output power  $P_4$  can be determined; in addition to the energy consumption of each module, factors, such as the impact of the natural wind field and environmental magnetic interference, will also indirectly lead to extra power generation. This part of power cannot be measured directly and can be regarded as the error term of the endurance time model, which is set as the environmental impact power  $P_5$ . The relationship between the power of each module and the total hovering output power of the UAV is

$$P_{all}(T) = \sum_{i=1}^5 P_i(T). \quad (2)$$

### 2.2.1. Module Power Data Measurement

In order to obtain the working power data of each module, using specific measuring equipment, the group designed a corresponding wiring measurement method. The selected power measuring equipment includes a UAV power system test bench (type LY-30, Tianjin Lingyi Flying Co., Ltd. Tianjin, China), DC power supply (type LP220DE), and high-precision external dynamometer (type ZFT-8), of which the parameters are shown in Table 2.

**Table 2.** Measuring equipment parameters.

Main Equipment	Type	Precision	Power Supply Form
DC power power	LP220DE	Voltage regulation error: $\leq 0.01\% + 2 \text{ mA}$	AC 220 V $\pm 10\%$
Motor test bench	LY-30	Tension sensor: $\leq 0.05\% \pm 10 \text{ g}$ Voltage sensor: $\leq 1.0\%$ current sensor: $\leq 1.0\% + 0.1 \text{ A}$	AC 220 V
Dynamometer	ZFT8	Power sensor: $\leq 0.01\%$	DC 4.5 V–150 V

The power data of each module are obtained by mounting the motor and ESC on the motor test bench and connecting the ESC power and signal cables to the corresponding interface of the test bench. The output voltage of the power supply is set to 22.2 V (standard operating voltage of the motor), and the remaining equipment is wired, as shown in Figure 2. The data of  $P_1$  and  $P_3$  are, respectively, recorded by the memory of the motor test bench and the power meter, while  $P_2$  is expressed as the difference between the values of the two power meters connected to the input and output of the power divider. When the test starts, the PWM signal is output from the signal terminal of the motor test bench, the throttle is controlled to increase evenly in the range of 0–100% at 5% intervals, and the output power value of each module is recorded at each throttle position.

Under the same motor pull, the difference between the total power of the UAV ground test and the total hovering output power is the environmental impact power  $P_5$ . To obtain the power data of  $P_5$ , eight nodes of motor pull values are evenly selected in the interval of the UAVs take-off mass pull (limited by the empty aircraft mass, the minimum motor pull is chosen as 1.9 kg in the hover test), and the sum of module power corresponding to each node is available by ground measurement. Then, under the same motor output pull, the UAV is controlled to complete a five-minute stable hover, and the hovering output power is recorded by the dynamometer connected to the battery output and the difference

between the two is the environmental impact power under different load conditions. The power measurement results of each module are shown in Table 3.

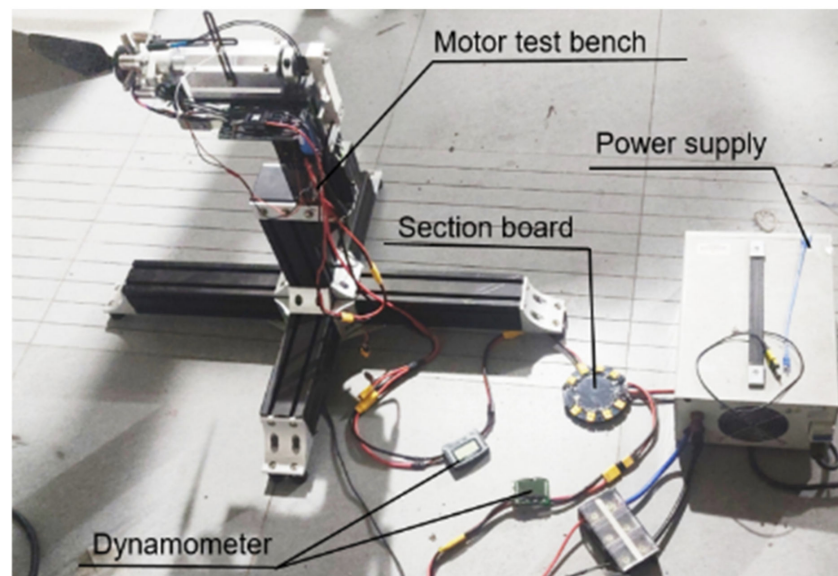


**Figure 2.** Device wiring physical diagram.

**Table 3.** Test module output power and proportion.

Motor Pull (kg)	Pull Curve (w)	Section Board (w)	Dynamometer (w)	Environmental Impact (w)
1.90	179.00/92.53%	6.38/3.30%	2.77/0.36%	29.55/3.82%
2.27	230.00/92.78%	6.64/2.68%	3.08/0.31%	41.97/4.23%
2.70	294.00/92.14%	6.64/2.68%	3.08/0.31%	41.97/4.23%
3.16	362.00/91.27%	8.11/2.04%	3.48/0.22%	102.50/6.46%
3.57	441.00/91.05%	9.26/1.91%	3.80/0.20%	132.50/6.84%
4.03	523.00/90.92%	11.55/2.01%	4.47/0.19%	158.30/6.88%
4.45	605.00/91.18%	15.42/2.32%	5.14/0.19%	167.20/6.30%
4.84	692.00/91.79%	17.31/2.30%	6.11/0.20%	172.30/5.71%

### 2.2.2. Module Output Power Function Fitting

Based on the module power test data, the power scatter plots of each module under different working pull are plotted, polynomial fitting of the curve is performed using the `cftool` tool of MATLAB, with 99% fitting accuracy as the standard, and the final results are shown in Figure 3 with careful consideration of fitting accuracy and model complexity.

### 2.2.3. Static Energy Consumption Module

The agricultural UAVs flight control is generally installed inside the airframe near the center of gravity of the whole aircraft. Due to the harsh field operation environment and poor heat dissipation conditions inside the airframe [20], the flight control power may take the maximum value within its power variation interval. Taking DJI N3 flight control as an example, its rated output power is 3.6–4.8 W, and in the subsequent modeling process, the flight control power is taken as 4.8 W.

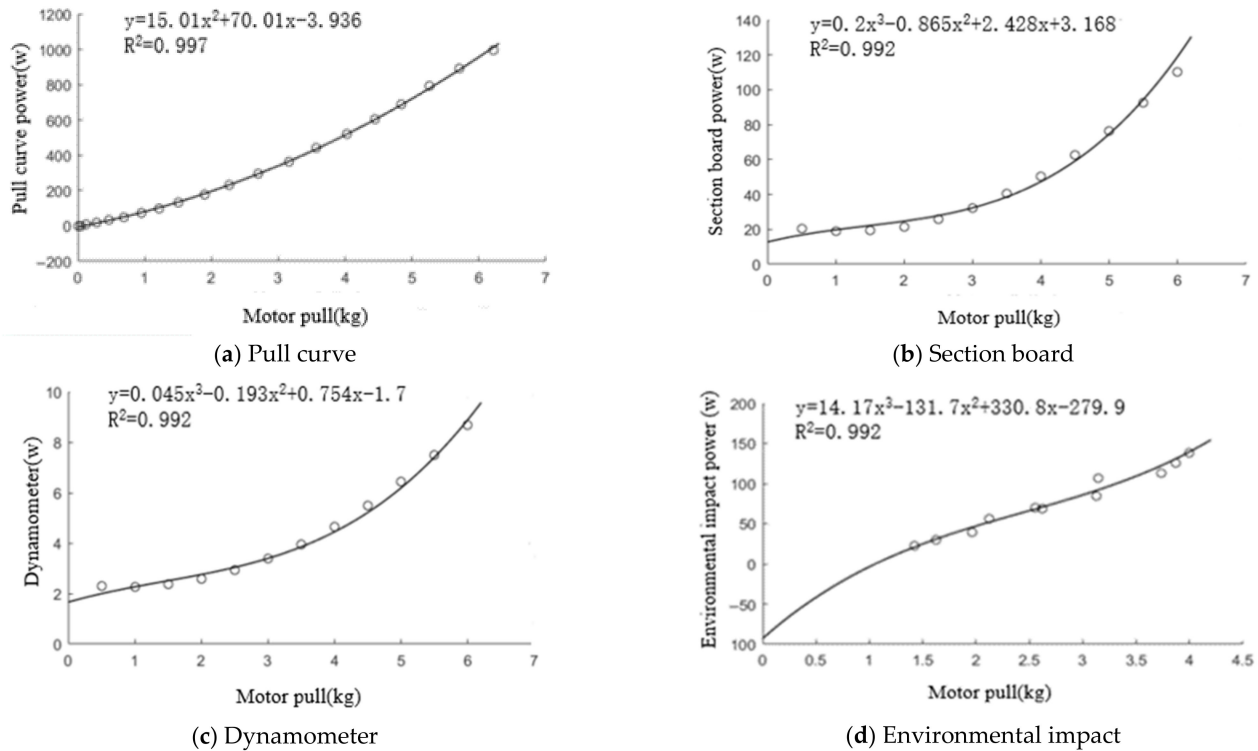


**Figure 3.** Module output power fitting results.

### 2.3. Endurance Evaluation Model of Agricultural UAVs

#### 2.3.1. Theoretical Analysis of the Evaluation Model

This paper takes a common electric drone as the research object, whose load distribution pattern and output power variation characteristics, modeling ideas, and data measuring methods have good generality among conventional rotary wing UAVs. The model takes the battery mass and operational load as input and the endurance time as output, and after substituting the power fitting function of each module, this model can be quickly established to provide theoretical data reference for its operational parameters configuration.

#### 2.3.2. Endurance Evaluation Model

From the literature [21,22], the hovering duration of the electric UAV can be expressed as

$$t = \frac{C_b - C_{min}}{I_b} \cdot \frac{60}{1000}. \quad (3)$$

$t$ —Hovering endurance time of drone;  $C_b$ —Nominal battery capacity;  $C_{min}$ —Minimum battery capacity;  $I_b$ —Battery discharge current.

According to the discharge characteristics of the power battery [23], the power consumption value of the UAV can be expressed as the integral of the hovering output power over the endurance time, i.e.,

$$E = \int_0^t P_{all}(T)d(t). \quad (4)$$

Subject to the development level of lithium battery technology, there is no significant difference in the energy density of ordinary high-capacity batteries (as shown in Table 4). To facilitate the calculation,  $e$  is set as a constant and takes the value of 200 wh/kg.

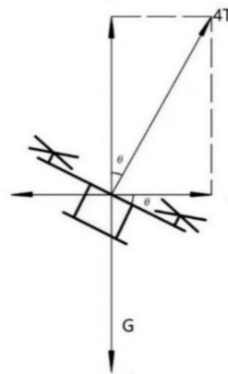
**Table 4.** Common high-capacity battery parameters.

Battery Brand	Capacity (mah)	Weight (kg)	Total Energy (wh)	Energy Density (wh/kg)
Kudian	16,000	2.7	555.2	205.6
DJI MG1	12,000	1.85	366.4	198.05
XAG P20	16,000	4.53	850	187.64
DJI T16	17,500	4.75	906	190.84

From the literature [24], in the actual operation of rotary wing UAVs, the remaining power should be higher than 15% to avoid damage to the battery cells from low voltage. After the UAV lands, the ratio of the remaining battery capacity to the nominal capacity is defined as the depth of discharge coefficient  $Y$ , whose value should be slightly higher than 15% and therefore is taken as 0.8. Then, the total battery energy is

$$E = W_3 \cdot e \cdot Y. \quad (5)$$

When the UAV is hovering at a fixed height, the dynamic balance relationship between the total motor output pull force and the take-off mass is always maintained. To simplify the model, the average pulling force of a single motor is expressed as 1/4 of the take-off mass of an electric quad-rotor UAV [25–27]. To ensure flight safety, the maximum take-off mass of the UAV must be limited, and enough power redundancy should be remained to maintain a stable flight at the limit. The angle between the motor pull axis and the body gravity axis is  $\theta$  when the UAV is flying horizontally at a constant speed, as shown in Figure 4.

**Figure 4.** Force Analysis of UAV.

At this time, the relationship between the pulling force of the motor and the gravity of the fuselage is  $W_T = 4 T \cdot \cos\theta$ . If the tilt angle is too large and the vertical component of the pulling force is less than the gravity of the fuselage, it will lead to a height drop during the flight or even a crash. The maximum tilt angle of current agri-drones is generally less than  $40^\circ$ . Taking this as a reference and then adding the influence of environmental factors, the ultimate tilt angle of the fuselage is set at  $45^\circ$ . The ratio of the vertical component of the motor pull to the total motor pull is the pull redundancy factor  $\eta$ , which is calculated to be 0.707. The product of this coefficient and the motor limit pull determines the upper limit of the UAV load capacity. In summary, the relational expression of the final range assessment model is

$$t = \frac{W_3 \cdot e \cdot Y}{P_{all} \left( \frac{1}{n} \sum_{i=1}^n W_i \right)}; \quad (6)$$

$$W_3 + W_4 \leq 0.707 \cdot T_{max}. \quad (7)$$

$t$ —Hovering time of drone;  $T$ —Average pulling force of single motor;  $W_1$ —Weight of the fuselage structure;  $W_2$ —Weight of power system;  $W_3$ —Battery weight;  $W_4$ —Workload weight;

$n$ —Number of rotors;  $e$ —Battery energy density;  $Y$ —Battery depth of discharge coefficient;  $T_{max}$ —Maximum motor test total pulling force;  $\eta$ —Pulling force redundancy coefficient.

### 2.3.3. Model Calculation Results

In order to provide comparative data for the model validation phase, when the endurance evaluation model is established, the Simulink tool of MATLAB is used to perform the theoretical calculation, and the corresponding calculation structure is shown in Figure 5. The module in it is the power fitting function of each component, containing two input parameters (battery mass and operational load) and one output parameter (endurance time). After substituting the specific energy consumption data of the AX-1000 UAV, calculation results are shown in Table 5 below.

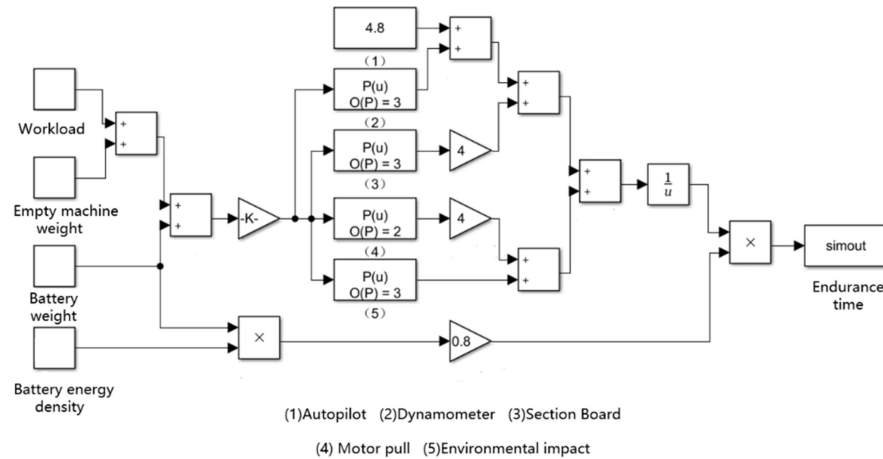


Figure 5. The structure diagram of the theoretical calculation model.

Table 5. Model verification experiment data.

Battery Weight (kg)	Payload (kg)	Test #2 (h)	Test #1 (h)	Test #3 (h)	Model Calculation Results (h)	Average Error Rate
0.70	0	0.203	0.203	0.202	0.203	0.164
0.70	2.00	0.137	0.135	0.135	0.136	0.499%
0.70	5.00	0.088	0.090	0.086	0.088	0.309%
0.70	7.00	0.070	0.072	0.070	0.072	1.458%
0.70	9.00	0.056	0.058	0.055	0.058	2.695%
1.50	0	0.366	0.368	0.364	0.366	0.039%
1.50	2.00	0.256	0.255	0.253	0.256	0.577%
1.50	4.00	0.194	0.195	0.191	0.194	0.309%
1.50	6.00	0.150	0.152	0.154	0.154	1.487%
1.50	8.44	0.115	0.116	0.115	0.118	2.678%
1.50	9.50	0.104	0.104	0.106	0.107	2.306%
2.36	0.50	0.452	0.449	0.450	0.449	0.668%
3.50	2.00	0.454	0.452	0.451	0.454	0.331%
3.50	4.00	0.350	0.352	0.350	0.356	1.458%
3.50	6.44	0.268	0.268	0.269	0.276	2.703%
3.50	7.50	0.244	0.244	0.242	0.249	2.293%
4.72	0.50	0.633	0.635	0.632	0.634	0.063%
5.50	2.00	0.550	0.552	0.550	0.559	1.427%
5.50	4.44	0.421	0.423	0.420	0.433	2.686%
5.50	5.50	0.383	0.385	0.383	0.392	2.289%
7.08	0.50	0.706	0.702	0.703	0.709	0.786%
7.50	2.44	0.575	0.577	0.577	0.592	2.695%
7.50	3.50	0.522	0.524	0.524	0.535	2.306%
9.44	0.50	0.723	0.725	0.723	0.743	2.690%
9.50	1.50	0.662	0.660	0.662	0.677	2.301%

### 3. Model Validation

To verify the reliability and accuracy of the model effectively, the AX-1000 UAV was taken as the validation example, and several testing points were evenly selected within the interval of its battery mass and operational load variation, and the UAV was configured according to the corresponding parameters of the testing points. After completing the hovering endurance test, the model effect was analyzed and evaluated by calculating the error rate between the actual test endurance and the theoretical endurance of the model.

#### 3.1. Calculation Method of Equivalent Endurance

In the model verification experiments, if the endurance time corresponding to the complete discharge of batteries is recorded in a conventional way, the performance difference between individual batteries will cause a certain error in the test results. The test shows that the output power of the UAV is basically constant during the hovering discharge process (as shown in Figure 6), so the hovering time can be measured by applying the equivalent endurance concept as follows: the discharge energy of a single battery is 401.28 Wh and the measured hovering output power of the UAV (single battery) is 766.71 W. By calculating the ratio of the two, the equivalent endurance time is 0.523 h.

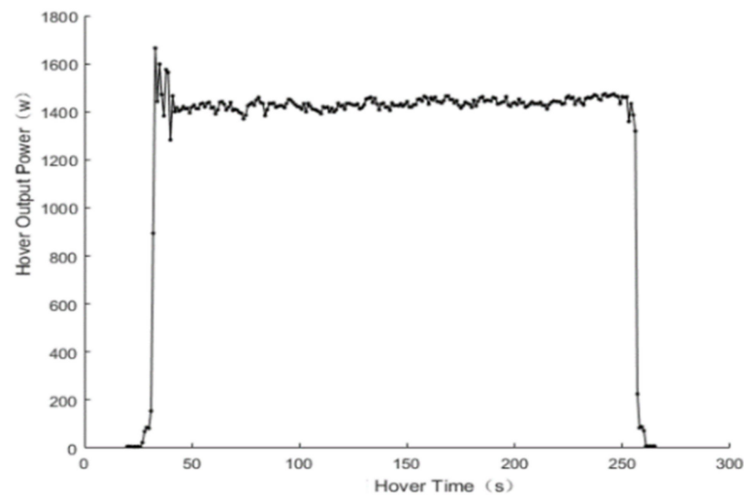


**Figure 6.** UAV hovering output power.

To verify the feasibility of the scheme, a hovering test in a fully discharged state was carried out under the above configuration, and the average voltage of the single-chip cell was 3.78 V after landing. The measured endurance time was 0.508 h, with a relative error of 2.87%. In addition, since the method is applied to both theoretical model calculation and verification experiment endurance calculation, its error does not affect the verification results.

#### 3.2. Distribution of Verification Points on the Endurance Surface

The maximum pulling force of the AX-1000 UAV supporting motor is 6 kg and combined with Equation (7), the maximum take-off mass is 17 kg, so the sum of the maximum battery and operational load of this model is 12 kg. The actual hovering test shows that when the total load mass reaches 11.5 kg, the UAV hovering drift is serious and cannot meet the experimental requirements, so the maximum total load of the surface verification point is set to 11 kg. The minimum battery mass is 0.7 kg; therefore, the surface area, with a total load lower than 0.7 kg, cannot be verified. Based on the above, the current range surface verification points are 27 in total, and the distribution is shown in Figure 7.

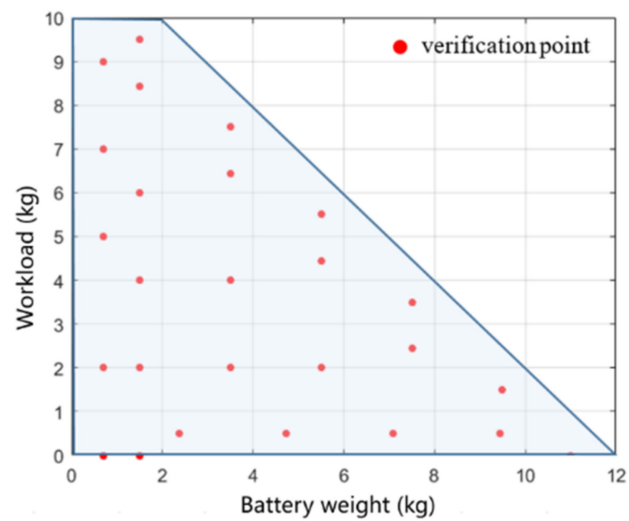


**Figure 7.** Distribution of verification points.

### 3.3. Verification Point Endurance Test

The model validation experiment was completed on the lawn of Lotus Garden in Qilin District, South China Agricultural University. During the experiment, the weather was clear, the ambient temperature was below 30 degrees, and the ground wind speed was between 1 and 3 m/s, which satisfied the flight test conditions. By changing the number of battery mountings and the mass of the operational load (replaced with weights of the same mass), the configuration of parameters corresponding to each sampling point was achieved, respectively. Thereafter, the UAV was maneuvered for a five-minute hovering test, and the hovering output power data was recorded by the power meter throughout the test, as shown in Figure 8. The experiment was repeated three times under each parameter configuration for a total of 75 experiments. Stable output power data of about three minutes were extracted from each set of data, and the average output power and the endurance time were calculated through equivalent endurance measurement, and then the calculated results were compared with the model output under the same configuration to calculate the relative error rate between them.



**Figure 8.** UAV hovering endurance test.

### 4. Results and Discussion

#### 4.1. Verification of Experimental Results

The results of verification experiments are presented in Table 5.

#### 4.2. Error Analysis

As seen from the data in Table 5, the overall accuracy of the model is high, and the maximum error value at the validation point is 2.7%. The error values of each validation point are marked on the model surface in the form of error bars, and the results are shown in Figure 9a. From the figure, it can be seen that the model error gradually increases as the total mass of the load increases.

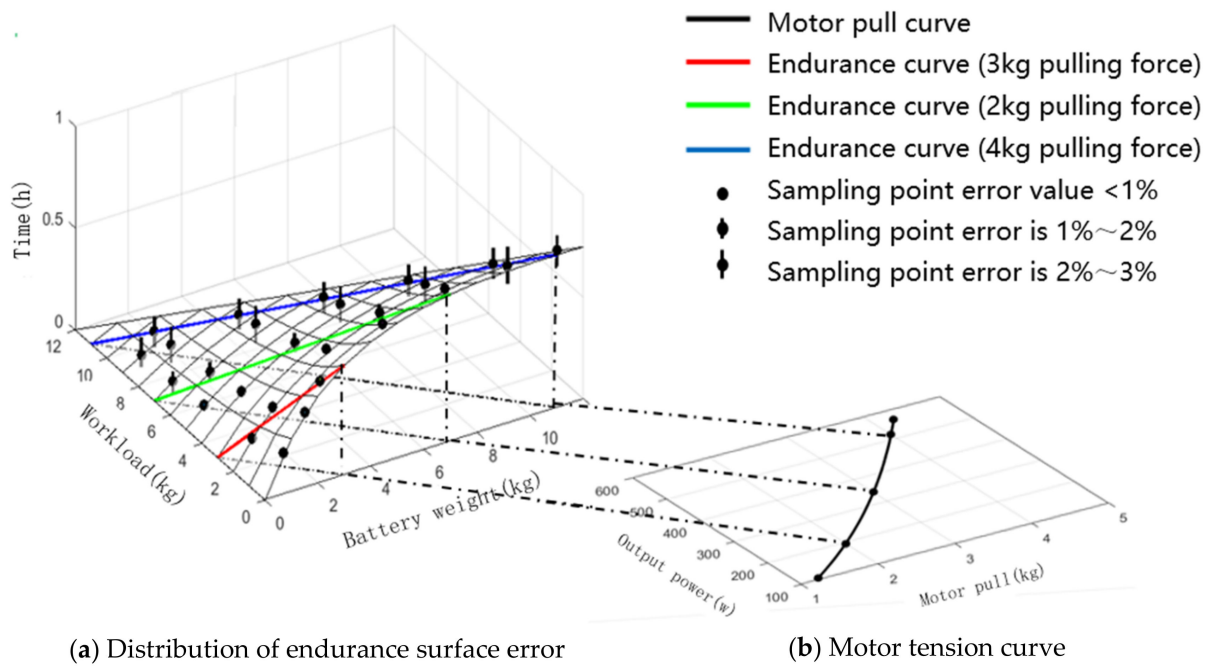


**Figure 9.** Model error analysis diagram. Note: The first and last ends of the pulling force curve correspond to the pulling force working point of the UAV under no-load and maximum take-off mass.

The current error distributing characteristics are mainly related to the motor pull curve, which characterizes the correspondence between output pull and output power of the motor. With the pulling force changing, the UAV working state changes accordingly, so the motor output pull can be defined as the pulling force working point. As can be seen from Equation (8), when the sum of the battery and operating load mass is a constant value, both the motor hovering tension working point  $T$  and the corresponding hovering output power  $P_{all}(T)$  in the model are constant, and the model expression becomes

$$t = \frac{W_3 \cdot e \cdot Y}{P_{all}(T)} \tag{8}$$

At this point, there is a directly proportional relationship between battery life and battery mass. In Figure 9a, the endurance timelines corresponding to the three pulling force working points are all straight in space, and the slope coefficient  $k$  is expressed as

$$k = \frac{e \cdot Y}{P_{all}(T)} \tag{9}$$

When the motor pull working point moves up and the hovering power increases, the slope of the endurance curve gradually decreases. Accumulating the corresponding endurance curves in space throughout the change interval of the tension operating point,

the corresponding relationship between the formed endurance time surface and the motor tension curve is shown in Figure 9.

In the hovering state, when affected by environmental factors such as external wind field, magnetic field interference, and GPS signal drift, the UAV maintains a stable hover by adjusting the output pull of each motor. In this process, the hovering power varies with the deviation of the tension working point. After being influenced by the environment, the tension working point offset is set as 0.1 kg. If the current tension working point is 2 kg or 4 kg, the corresponding power offset is 47.2 W or 96 W.

According to the hovering power change law mentioned above, the motor power variation corresponding to the low-tension area is significantly lower than that of the high-tension area when the tension working point offset is the same. Combined with Figure 9b, in low-tension areas where the workload is less, the power deviation, resulting from the offset of the tension working point caused by environmental effects, is smaller, so the model accuracy in this region is higher. On the contrary, in high-tension areas, the power deviation caused by environmental influences is larger, leading to the reduction of model accuracy.

The output power deviation, affected by the environment, is compensated by the environmental influence power  $P_5$  in the model. Under high-load conditions, the hovering output power of the UAV fluctuates greatly, and the accuracy of the  $P_5$  function fitting curve decreases accordingly, resulting in a decrease in model accuracy. However, in the daily operation condition, the working points of the motor pull of agricultural UAVs are all located in the low and middle areas, so the loss of accuracy in the high-load area basically has no impact on the practical application of the model. To further improve the accuracy of the model, it is necessary to increase the amount of test data of  $P_5$  to improve the fitting accuracy of the power function of the module.

#### 4.3. Model Application

In the field operation process of agricultural UAVs, in order to ensure a uniform spraying effect, the spraying flow rate is generally constant [28]. Assuming that the spraying flow rate is a definite value  $Q$ , the effective spraying time  $t_1$  can be calculated according to the workload and spraying flow rate, and the corresponding relationship is

$$t_1 = \frac{W_3}{Q}. \quad (10)$$

The endurance time of the UAV is determined by the workload and battery mass together, and if the two parameters are poorly matched, it will have a negative impact on the operating efficiency [29,30]. Currently, the battery configuration of agricultural drones is relatively small, and the workload is mainly water tank liquid, the mass of which is easy to adjust. Therefore, the matching between the two parameters is mainly achieved by adjusting the workload mass.

Taking the AX-1000 UAV as an example, assuming that the battery mass and spraying flow are constant, and substituting the fuselage parameters into the endurance evaluation model, the endurance time expression can be obtained as

$$t = \frac{160W_3}{P_{all}(\frac{5+W_3+W_4}{4})}. \quad (11)$$

The endurance time here is the space curve, and the effective spraying time is the space diagonal line. Limited by the maximum load capacity, the workload variation interval of both timelines is the same. For a given battery configuration, the two lines are in the same plane and have an intersection, as shown in Figure 10.

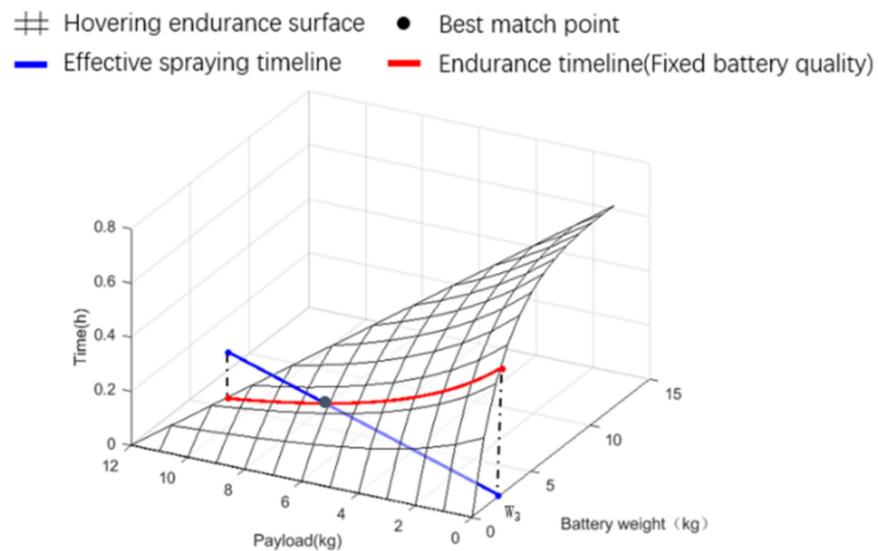


**Figure 10.** Schematic diagram of model application. Note: This is only a simple example of the application effect of the model, so the impact of the change in the remaining amount of medicine during the spraying process on the hovering time has not been considered. The actual spraying operation will change the slope of the original endurance curve, but its essence remains the same, and the matching mechanism between the battery and the operating load is not affected.

As can be seen from Figure 10, the effective spraying time to the left of the intersection is longer than the endurance time, which means that the spraying operation has not yet ended, while the UAV power has been exhausted, at which time it is necessary to reduce the operating load and shorten the spraying time. The situation is exactly the opposite on the right side of the intersection; that is, when the spraying work is over, the UAV still has more power left. In this case, it is necessary to increase the operating load and extend the spraying time. If the return power is not considered, the optimal configuration point of the workload in the figure will be the intersection of the two lines. Taking the 2.36 kg battery (mass of a single battery) and 0.5 L/min (standard working flow rate of the nozzle) as an example, the corresponding best operation mass is 6.173 kg, when the endurance and effective spraying time are both 0.214 h. If part of the return power needs to be reserved, the workload can be moderately reduced on the basis of the best configuration point, according to the distance of the return trip.

## 5. Conclusions

(1) Under the standard take-off configuration, the part with the highest mass proportion of the UAV is the workload (40.45%), and the module with the highest output power is the motor pull power (91.12%), so the main influencing factor of UAV mass distribution system is the workload, and that of the UAV power distribution system is the motor tension.

(2) This article creatively proposes a rapid evaluation model for the endurance of agricultural UAVs, validated by hovering tests. The results show that the maximum error of the verification point is 2.73%, and the model achieves high accuracy. Both the modeling idea and the fast measurement method of module power are universal.

(3) The endurance evaluation method can be applied to guide the reasonable configuration of the battery and workload of agricultural drones. Taking AX-1000 UAV as an example, without regard to the remaining return power, the optimal working load is 6.173 kg under the conditions of a 2.36 kg battery and 0.5 L/min spraying flow rate, and both the endurance time and effective spraying time are 0.214 h.

**Author Contributions:** Conceptualization, H.W.; methodology, B.L.; software, L.C.; validation, X.W.; formal analysis, B.L. and X.H.; investigation, B.L.; resources, J.L.; data curation, B.L. and X.H.; writing—original draft preparation, B.L.; writing—review and editing, B.L. and H.M.; supervision, Z.Z.; project administration, H.M.; funding acquisition, J.L. and J.X. All authors have read and agreed to the published version of the manuscript.

**Funding:** This research was funded by the Key Project of the Natural Science Foundation of Guangdong Province (2021A1515010736) and the Guangzhou key research and development project/202206010164.

**Data Availability Statement:** Not applicable.

**Conflicts of Interest:** The authors declare no conflict of interest.

## References

- Guang, B.; Xin, S.; Shuang, C.; Wen, Q. Multiple UAV Cooperative Trajectory Planning Based on Gauss Pseudospectral Method. *J. Astronaut.* **2014**, *35*, 10–22. [[CrossRef](#)]
- Zhang, D.; Lan, Y.; Chen, L.; Wang, X.; Liang, D. Current Status and Future Trends of Agricultural Aerial Spraying Technology in China. *Nongye Jixie Xuebao/Trans. Chin. Soc. Agric. Mach.* **2014**, *45*, 53–59.
- Zhang, B.; Zhai, C.; Li, H.; Han, S. Development Status Analysis of Precision Pesticide Application Techniques and Equipments. *J. Agric. Mech. Res.* **2016**, *4*, 1–5.
- Tang, W.; Song, B.; Cao, Y.; Yang, W. Preliminary Design Method for Miniature Electric-Powered Vertical Take-off and Landing Unmanned Aerial Vehicle and Effects of Special Parameters. *Acta Aeronaut. Astronaut. Sin.* **2017**, *38*, 120–133. [[CrossRef](#)]
- Pei, Y. *Analysis of the Mechanical Characteristics of the Transmission System of a Heavy-Duty Four-Rotor UAV*; Shenyang University of Technology: Shenyang, China, 2019.
- Zhang, D.; Li, J.; Wang, Y. Development Status and Trends of High-Altitude and Long-Endurance UAVs. In Proceedings of the 2014 (Fifth) China UAV Conference, Beijing, China, 9 July 2014.
- Zhou, Z.; Ming, R.; Zang, Y.; He, X.; Luo, X.; Lan, Y. Development Status and Countermeasures of Agricultural Aviation in China. *Trans. Chin. Soc. Agric. Eng.* **2017**, *33*, 1–13. [[CrossRef](#)]
- He, X. Improving Severe Draggling Actuality of Plant Protection Machinery and Its Application Techniques. *Trans. Chin. Soc. Agric. Eng.* **2004**, *20*, 13–15. [[CrossRef](#)]
- Xie, C.; Duan, Y.; Xu, W.; Zhang, H.; Li, X. A Low-Cost Neutral Zinc–Iron Flow Battery with High Energy Density for Stationary Energy Storage. *Angew. Chem.* **2017**, *129*, 15149–15153. [[CrossRef](#)]
- Zeng, H.; Wang, Y.; Zhang, Z. Mathematical Derivation and Analysis of Factors Affecting the Performance of Permanent Magnet Brushless DC Motors. *J. Liaoning Univ. Technol. Nat. Sci. Ed.* **2020**, *40*, 29–32.
- Lian, H.; Zhang, C.; Li, G. Overview of the Performance of Long-Endurance Multi-Rotor Drones. Proceedings of OSEC First Ordnance Engineering Conference, Chongqing, China, 15–16 September 2017.
- Guo, Y.; Yuan, H.; He, X. Development Status and Prospect Analysis of My Country’s Agricultural Aviation Plant Protection. *China Plant Prot. Guide* **2014**, *34*, 78–82.
- Thibbotuwawa, A.; Nielsen, P.; Zbigniew, B.; Bocewicz, G. Energy Consumption in Unmanned Aerial Vehicles: A Review of Energy Consumption Models and Their Relation to the UAV Routing. In *Information Systems Architecture and Technology: Proceedings of 39th International Conference on Information Systems Architecture and Technology—ISAT 2018*; Świątek, J., Borzemski, L., Wilimowska, Z., Eds.; Springer International Publishing: Cham, Switzerland, 2019; pp. 173–184.
- Liu, Z.; Sengupta, R.; Kurzhanskiy, A. A Power Consumption Model for Multi-Rotor Small Unmanned Aircraft Systems. In Proceedings of the 2017 International Conference on Unmanned Aircraft Systems (ICUAS), Zhuhai, China, 27–29 October 2017; pp. 310–315.
- Traub, L.W. Validation of Endurance Estimates for Battery Powered UAVs. *Aeronaut. J.* **2013**, *117*, 1155–1166. [[CrossRef](#)]
- Tang, W.; Song, B.; Cao, Y. The Overall Design Method of Micro Electric Vertical Take-off and Landing UAV and the Influence of Special Parameters. *Acta Aeronaut. Sin.* **2017**, *30*, 115–128.
- An, S.; Liu, X.; Hou, K. Establishment of the Dynamic Model of the Electric Power System of a Slight UAV. *J. Harbin Univ. Sci. Technol.* **2020**, *3*, 33–39.
- Jin, J.; Zhu, Y.; Zeng, S. Research on the Endurance of Small Multi-Rotor Drones. *Comput. Knowl. Technol.* **2017**, *13*, 197–199.
- Liu, F.; Ma, X. Research for Improving the Endurance Performance of Minitype Electric-Powered UAV. *Flight Dyn.* **2010**, *5*, 13–15. [[CrossRef](#)]
- Lu, J.; Cen, H. The Application Status and Problems of Small Drones in Agricultural Plant Protection. *Use Maint. Agric. Mach.* **2014**, *5*, 123.
- Liu, S.; Li, Q.; Lu, N. A Method for Estimating the Endurance of Micro Electric Drones. In Proceedings of the 26th China Control and Decision Conference, Zhangjiajie, China, 31 May–2 June 2014.
- Lin, J.; Lan, Y.; Ouyang, F.; Li, J.; Chen, P. Construction and Experimental Verification of Power Consumption Model for Multi Rotor Agricultural UAV. *J. Agric. Mech. Res.* **2020**, *42*, 149–155.

23. Zhu, X.; Zhu, J.; Wang, J.; Gan, Z.; Meng, C. Experimental Study on Long Cycling Performance of NCM523 Lithium-Ion Batteries and Optimization of Charge-Discharge Strategy. *J. Therm. Sci.* **2020**, *29*, 1180–1192. [[CrossRef](#)]
24. High Temperature Operation Battery Maintenance of Plant Protection Drone. *Agric. Mach.* **2020**, *873*, 56.
25. Li, J.; Zhan, Y.; Ou, Y.; Li, Y.; Lan, Y. Rotor Spacing Optimization and Energy Consumption Test of a Multi-Wing Single-Arm Tandem Electric UAV. *Trans. Chin. Soc. Agric. Eng.* **2019**, *35*, 87–95.
26. Azaceta, E.; García, S.; Leonet, O.; Beltrán, M.; Gómez, I.; Chuvilin, A.; Mainar, A.R.; Blazquez, J.A.; Knez, M. Particle Atomic Layer Deposition as an Effective Way to Enhance Li-S Battery Energy Density. *Mater. Today Energy* **2020**, *18*, 100567. [[CrossRef](#)]
27. Li, J.; Zhou, Z.; Lan, Y.; Hu, L.; Zang, Y.; Liu, A.; Luo, X.; Zhang, T. Distribution of Canopy Wind Field in Pollination Operation of Rotary-Wing UAV. *Trans. Chin. Soc. Agric. Eng.* **2015**, *31*, 85–94.
28. Li, J.; Luo, H.; Zhu, C.; Li, Y.; Tang, F. Research and Implementation of Combination Algorithms about UAV Spraying Planning Based on Energy Optimization. *Trans. Chin. Soc. Agric. Mach.* **2019**, *50*, 106–115.
29. Xu, B.; Chen, L.; Tan, Y.; Xu, M. Study on the Minimum Energy Trajectory Planning Algorithm for Plant Protection Drones with Multiple Sorties. *Trans. Chin. Soc. Agric. Mach.* **2015**, *46*, 43–49.
30. Fan, Y.; Shen, K.; Wang, D.; Zhai, C.; Zhang, H. Optimal Path Planning of Energy Consumption for UAV Mountain Operations Based on Simulated Annealing. *Algorithm Trans. Chin. Soc. Agric. Mach.* **2020**, *51*, 34–41.